Kinetically Relevant Steps and H₂/D₂ Isotope Effects in Fischer−Tropsch Synthesis on Fe and Co Catalysts

Manuel Ojeda,[†] Anwu Li,[†] Rahul Nabar,[‡] Anand U. Nilekar,[‡] Manos Mavrikakis,*[‡] and Enrique Iglesia*[†]

Department of Chemical Engineering, University of California, and Division of Chemical Sciences, E.O. Lawrence Berkeley National Laboratory, Berkeley, California 94720, United States, and Department of Chemical and Biological Engineering, University of Wisconsin, Madison, Wisconsin 53706, United States

H₂/D₂ isotope effects on Fischer−Tropsch synthesis (FTS) rate and selectivity are examined here by combining measured values on Fe and Co at conditions leading to high C_{5+} yields with theoretical estimates on model Fe(110) and Co(0001) surfaces with high coverages of chemisorbed CO (CO*). Inverse isotope effects (r_H/r_D < 1) are observed on Co and Fe catalysts as a result of compensating thermodynamic (H₂ dissociation to H*; H* addition to CO* species to form HCO*) and kinetic (H* reaction with HCO*) isotope effects. These isotopic effects and their rigorous mechanistic interpretation confirm the prevalence of H-assisted CO dissociation routes on both Fe and Co catalysts, instead of unassisted pathways that would lead to similar rates with H₂ and D₂ reactants. The small contributions from unassisted pathways to CO conversion rates on Fe are indeed independent of the dihydrogen isotope, as is also the case for the rates of primary reactions that form CO_2 as the sole oxygen rejection route in unassisted CO dissociation paths. Isotopic effects on the selectivity to C_{5+} and CH_4 products are small, and D₂ leads to a more paraffinic product than does H₂, apparently because it leads to preference for chain termination via hydrogen addition over abstraction. These results are consistent with FTS pathways limited by H-assisted CO dissociation on both Fe and Co and illustrate the importance of thermodynamic contributions to inverse isotope effects for reactions involving quasi-equilibrated H₂ dissociation and the subsequent addition of H* in hydrogenation catalysis, as illustrated here by theory and experiment for the specific case of CO hydrogenation.

1. Introduction

Fischer−Tropsch synthesis (FTS) is widely used to produce clean fuels from synthesis gas (H₂/CO).[1,2] Iron-based oxides are commonly used as catalyst precursors.[3] FTS involves polymerization of CH_x* monomers or their reaction with CO* (where * denotes an active site). The mechanism first proposed by Fischer and Tropsch (CO dissociation and subsequent carbon hydrogenation) is often assumed as the prevalent route for monomer formation,[4] but controversies remain about whether CH_x* species form from CO that dissociates before or after the addition of one or more H-atoms.[5−9] We have recently provided experimental and theoretical support for two parallel CO activation pathways: direct dissociation with subsequent H* reactions with C*, and H-addition to CO* before dissociation with C−O cleavage of partially hydrogenated species to form CH_x* and OH* species on Fe-based catalysts.[10] On Co-based catalysts, FTS occurs predominantly via CO dissociation after H-addition. Even on Fe-based catalysts, H-assisted CO activation predominates at practical FTS conditions (500−550 K, 2−4 MPa, H₂/CO = 1−2), and direct dissociation pathways contribute significantly only at very low H₂/CO ratios.

Hydrogen atoms formed via H₂ dissociation are involved in all elementary steps in H-assisted CO dissociation pathways, but participate in the unassisted routes only after CO dissociation to form C* and O* species. Therefore, H₂/D₂ kinetic and thermodynamic isotope effects can probe the involvement of H-atoms in specific elementary steps within catalytic sequences, because rate and equilibrium constants for these elementary steps depend on isotopic identity.

Kinetic isotope effects (KIE, r_H/r_D) have been reported for CO hydrogenation on several Ni, Ru, and Co catalysts, often with contradictory conclusions. H₂/D₂ isotope effects were near unity for CH_4 formation from H₂−CO on Ni/ZrO₂ at ambient pressures (400−500 K; 75 kPa H₂(D₂); 25 kPa CO),[11,12] suggesting that CO dissociation is the sole kinetically relevant step and that C* and O* species formed are rapidly scavenged by hydrogen in subsequent quasi-equilibrated steps. These mechanistic conclusions can be rendered equivocal by compensating kinetic and thermodynamic isotope effects.[13] In contradiction with these data, Ni/SiO₂ gave inverse kinetic isotope effects (r_H/r_D = 0.85)[14] at nearly identical conditions (475 K; 75 kPa H₂(D₂); 25 kPa CO), leading to the alternate proposal that H* addition to CH* limits methanation rates.

Similar contradictions prevail on Ru catalysts with normal KIE values (1.2−1.4) on Ru powder (310−385 K; 8 kPa H₂(D₂); 8 kPa CO):[15] no isotope effect on Ru/Al₂O₃ in one study (475−540 K; 75 kPa H₂(D₂); 25 kPa CO)[11,12] and inverse isotope effects (0.7) in another one (450−525 K; 75 kPa H₂(D₂); 25 kPa CO).[16] In all cases, reaction conditions led to the predominant formation of CH_4, making conclusions possibly irrelevant for the conditions and mechanisms of FTS, which involves significant chain growth and much higher pressures (1−3 MPa).

Inverse H₂/D₂ kinetic isotope effects (r_H/r_D = 0.7−0.8 range) during methanation (513 K, 0.07 MPa H₂(D₂); 0.03 MPa CO)[17]

* Corresponding authors. E-mail: iglesia@berkeley.edu (E.I.), manos@engr.wisc.edu (M.M.).
[†] University of California.
[‡] University of Wisconsin.

and FTS (473 K, 1.30 MPa $H_2(D_2)$; 0.67 MPa CO)[18] on Co have been explained by a combination of inverse thermodynamic effects for dissociative hydrogen adsorption and normal kinetic isotope effects for C–H bonds formed in transition states leading to CH* or CH_2* species.[19] C_{5+} selectivities were larger for D_2/CO than H_2/CO reactants, indicating that KIE values are smaller for chain growth than methanation steps. Inverse H_2/D_2 isotopic effects have also been reported on Fe catalysts[20] ($r_H/r_D = 0.85$; 543 K; 0.48 MPa $H_2(D_2)$; 0.72 MPa CO) and explained also by compensating effects of inverse thermodynamic effects for hydrogen dissociation and normal isotope effects for C–H bond formation. To our knowledge, none of these KIE values have been estimated from theoretical methods for the elementary steps claimed to be responsible for the values measured.

Here, we report the isotopic effects on rates and selectivities on state-of-the-art Fe–Zn–K–Cu catalysts[19] at conditions leading to significant C_{5+} selectivities (82–87%, CO_2-free basis) and compare them with similar effects that we have measured on Co catalysts.[18] These inverse isotope effects are interpreted in terms of compensating thermodynamic and kinetic isotope effects using a rigorous mechanistic interpretation of measured rate data combined with first-principle theoretical calculations on CO-saturated Fe(110) and Co(0001) model surfaces. These theoretical estimates indicate that measured inverse isotope effects reflect the prevalence of secondary thermodynamic isotope effects resulting from atoms and chemical bonds not directly involved in the kinetically relevant H-assisted CO dissociation step. The mechanistic origins of these effects are similar for FTS reactions on Co and Fe catalysts, consistent with the involvement of a common sequence of elementary steps. H_2–D_2 effects on chain growth probabilities are weak, with D-atoms very slightly increasing the selectivity to longer chains and leading to a small preference for chain termination by H-addition over H-abstraction. No H_2–D_2 isotope effects were found for rates of CO_2 formation via direct pathways, which involve the scavenging of O* atoms formed exclusively in direct dissociation of chemisorbed CO. The rate of formation of CO_2 via readsorption of H_2O and secondary CO–H_2O reactions on Fe showed a normal isotope effect. The measured isotope effects and their theoretical interpretations are consistent with the kinetic relevance of H-assisted CO dissociation steps leading to the exclusive formation of H_2O as the oxygen rejection path in FTS reactions on Fe and Co catalysts. On Fe, smaller contributions to measured rates from direct CO dissociation routes that form CO_2 as the oxygen carrier showed no H_2/D_2 isotope effects for the term in the rate equation corresponding to this route, consistent with the absence of chemisorbed hydrogen in the steps responsible for its rate parameters.

2. Methods

2.1. Catalyst Preparation. Fe–Zn oxide precursors were prepared by coprecipitation of mixed oxyhydroxides at a constant pH of 7 from mixed aqueous solutions of $Fe(NO_3)_3$ (Aldrich, 99.9%, 3.0 M) and $Zn(NO_3)_2$ (Aldrich, 99.9%, 1.4 M) using $(NH_4)_2CO_3$ (Aldrich, 99.9%, 1.0 M). Detailed procedures are reported elsewhere.[19] The precipitated powders (∼30 g) were washed with deionized water, dried at 393 K overnight in ambient air, and treated in flowing dry air (Praxair, UHP, 1.67 cm^3 s^{-1}) by increasing the temperature to 623 K at 0.167 K s^{-1} and holding for 1 h. Cu and K were introduced onto Fe–Zn oxide powders by incipient wetness impregnation with aqueous $Cu(NO_3)_2$ (Aldrich, 99.99%) and K_2CO_3 (Aldrich, 99.99%) solutions. The Zn/Fe, K/Fe, and Cu/Fe nominal atomic

ratios were 0.1, 0.02, and 0.01, and the surface area (Brunauer–Emmett–Teller) measured from N_2 physisorption at its normal boiling point was 65 m^2 g^{-1}.[3]

2.2. Fischer–Tropsch Synthesis Rates and Selectivities. H_2/D_2 kinetic isotope effects were measured as a function of space velocity at 508 K and 2.14 MPa total pressure in a packed-bed reactor with plug-flow hydrodynamics. Synthesis gas streams (H_2/CO/N_2; D_2/CO/N_2; 62/31/7 vol %) were prepared by mixing H_2 (Matheson, UHP) or D_2 (Cambridge Isotope Laboratories, Inc., 99.8%) with a CO/N_2 mixture (Matheson, UHP, 82/18 molar ratio) and metered using electronic flow controllers. The catalyst was activated in the reactant stream for 1 h at 100 kPa total pressure by increasing the temperature from 298 to 423 at 0.167 K s^{-1} and from 423 to 543 at 0.017 K s^{-1}. The reactor was cooled to ∼470 K, and the pressure was then increased to 2.14 MPa. Next, temperature was increased to the desired value (508 K). These preparation and activation protocols led to hydrocarbon synthesis productivities among the highest reported on Fe-based catalysts.[19,21,22]

Reactant and product concentrations were measured by direct transfer of inlet or outlet streams into a gas chromatograph (Hewlett-Packard 5890 Series II) equipped with a 10-port sampling valve and two sample loops, which were simultaneously injected into a cross-linked methyl silicone capillary column (HP-1; 50 m × 0.32 mm; 1.05 μm film) and a packed column (Porapak Q; 15.2 cm ×0.318 cm); their respective effluents were analyzed by flame ionization and thermal conductivity detection. Hydrocarbon synthesis rates are reported as the number of moles of CO converted to hydrocarbons or CO_2 per g-atom of Fe in the catalyst per hour. Hydrocarbon selectivities are reported on a carbon basis as the percentage of the CO converted to hydrocarbons appearing as each product (CO_2-free basis). CO_2 selectivities are reported as the percentage of the CO converted appearing as CO_2.

The data cited here for isotope effects on FTS rates and selectivities on Co-based catalysts were measured using similar protocols, and the detailed data and procedures have been reported separately.[18]

2.3. Theoretical Analysis. All calculations were performed using DACAPO, a periodic self-consistent density functional theory (DFT)-based total-energy code[23,24] utilizing the close-packed facets of Fe(110) and Co(0001) as model surfaces. The closest-packed Fe(110) and Co(0001) facets were selected for DFT calculations because they accurately represent the predominant low-index planes prevalent in the large crystallites used in the experiments. We do not consider that alternate structures are required for CO activation (e.g., high index facets,[25–27] carbided surfaces[28]), as we have shown in our previous FTS studies.[10] These model systems consisted of a four-layer metal slab, repeated periodically in a supercell geometry with five equivalent layers of vacuum between any two successive metal slabs. A 2 × 2 surface unit cell was used, and the top two layers of the slab were allowed to relax. In each unit cell, two CO molecules were treated as spectators, to simulate the high CO-coverage Fe or Co surfaces present under realistic FTS conditions.[10] All adsorbed species, including spectator CO molecules, were allowed to relax during energy minimization and minimum energy path calculations. The generalized gradient approximation (GGA-PW91) described the exchange-correlation energy and potential self-consistently.[29,30] Temperature effects have been taken into account using calculations for entropic contributions. Pressure effects are not accounted for directly, yet the choice of CO coverage on the model surfaces is made to reflect the high coverages prevalent during

H₂/D₂ Isotope Effects in FTS on Fe and Co Catalysts

J. Phys. Chem. C, Vol. 114, No. 46, 2010 **19763**
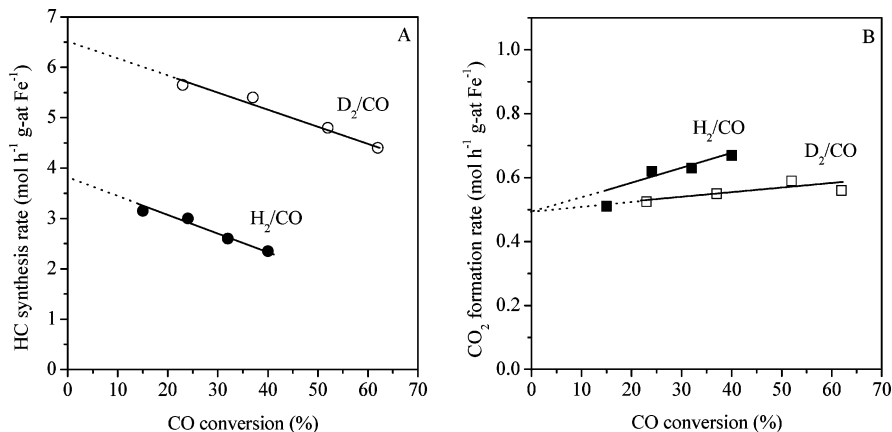
Figure 1. Hydrocarbon (HC) and CO_2 formation rate as a function of CO conversion with H_2/CO or D_2/CO over Fe−Zn−K−Cu catalyst (Zn/Fe = 0.1, K/Fe = 0.02, Cu/Fe = 0.01) at 508 K and 2.14 MPa.

steady-state FTS catalysis. Further details about the calculation protocols are included elsewhere.[10]
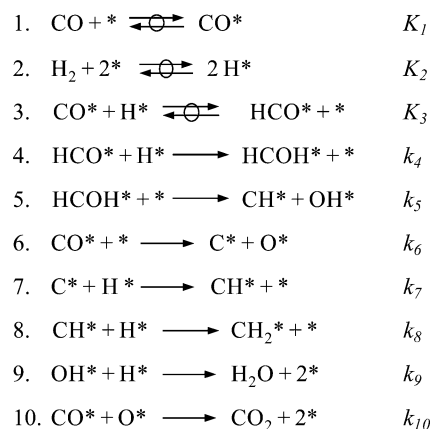
The effect of isotopic substitution was accounted for through its contributions to entropies as well as the energetics via zero-point energy (ZPE) corrections. As shown in the Appendix, the isotope effect per elementary step contains four contributions to the partition function: (i) translational, (ii) rotational, (iii) vibrational, and (iv) electronic. The last two contributions were calculated directly from the DFT-derived vibrational frequencies of relevant intermediates. Frustrated translations and rotations of adsorbed species are treated as special cases of vibrational modes. The only nonunity translational and rotational contributions to the partition function are for H_2(g) dissociation (see Appendix). All vibrational modes, except the imaginary one corresponding to the transition state of each elementary step, were accounted for in all ZPE and entropy calculations. Furthermore, all frequencies, including those for spectator CO*, were included in the ZPE corrections and entropy calculations. For H_2 dissociation (H_2 + 2* → 2H*), the initial state used was a H_2/D_2 molecule in the gas phase with a single vibrational mode calculated from DFT (4429 cm^{-1} (H) and 3134 cm^{-1} (D)). The rotational and translational contributions for this gas-phase molecule were calculated from standard formulas (see Appendix).

3. Results and Discussion

3.1. H₂/D₂ Isotope Effects on Hydrocarbon and CO₂ Formation Rate.
Figure 1 shows hydrocarbon synthesis and CO_2 formation rates as a function of the CO conversion level, which was varied by changing space velocity. Hydrocarbon synthesis rates decreased with increasing conversion because of reactant depletion, consistent with the rate equation derived below from a mechanistic sequence of elementary steps. Competitive adsorption of water and reactants, which are not included in this rate equation because rates were extrapolated to zero conversion, may also contribute to the observed decrease in reaction rates with increasing CO conversion.[31] Hydrocarbon formation rates were 2.0−2.5 times larger when D_2/CO was used instead of H_2/CO at all conversion levels (Figure 1A), indicating that FTS reactions on Fe-based catalysts exhibit inverse deuterium kinetic isotope effects (r_H/r_D < 1). These effects of the isotopic identity of dihydrogen reactants indicate that hydrogen species are involved in kinetically relevant steps and rule out unassisted dissociation of CO as the sole relevant step in FTS reactions.

Methane formation rates with H_2/CO and D_2/CO reactants (extrapolated to zero CO conversion to avoid reactant depletion

SCHEME 1: Elementary Steps for Hydrocarbons (CH₂* Species), Water, and Carbon Dioxide Formation from CO and H₂ with Fe-Based Catalysts

1. $CO + * \rightleftharpoons CO*$ — K_1
2. $H_2 + 2* \rightleftharpoons 2H*$ — K_2
3. $CO* + H* \rightleftharpoons HCO* + *$ — K_3
4. $HCO* + H* \longrightarrow HCOH* + *$ — k_4
5. $HCOH* + * \longrightarrow CH* + OH*$ — k_5
6. $CO* + * \longrightarrow C* + O*$ — k_6
7. $C* + H* \longrightarrow CH* + *$ — k_7
8. $CH* + H* \longrightarrow CH_2* + *$ — k_8
9. $OH* + H* \longrightarrow H_2O + 2*$ — k_9
10. $CO* + O* \longrightarrow CO_2 + 2*$ — k_{10}

or water inhibition effects) are 0.55 and 0.74 mol h^{-1} g-at Fe^{1-}, respectively. The corresponding KIE value (0.74) is larger than that for CO conversion to C_{5+} hydrocarbons (0.53; C_{5+} formation rates equal to 3.1 and 5.8 mol h^{-1} g-at Fe^{1-} with H_2/CO and D_2/CO reactants, respectively). These different isotope effects lead, in turn, to slightly higher C_{5+} selectivities when using D_2/CO instead of H_2/CO reactants. They also raise significant concerns about the use of isotope effects in methanation rates to infer mechanistic details of CO hydrogenation at conditions that favor chain growth (FTS).

Our previous studies have provided experimental and theoretical evidence for FTS pathways involving parallel H-assisted and unassisted routes for the kinetically relevant CO dissociation step on Fe-based catalysts (Scheme 1), leading to H_2O and CO_2 as the respective oxygen rejection routes.[10] Unassisted CO dissociation is followed by stepwise hydrogenation of C* to form FTS monomers (CH$_x$*) and reactions of O* with CO* to form CO_2. H-assisted routes involve H* addition before C−O bond-breaking to form monomers and OH* and sequential hydrogenation of OH* to form H_2O.

Measured CO_2 formation rates increased linearly as CO conversion increased with increasing residence time (Figure 1B), and the corresponding slope, a measure of the contribution of secondary CO_2-formation reactions to the overall rates,[32] is smaller for D_2/CO than for H_2/CO reactants. Rates extrapolated to zero CO conversion levels, which reflect the rate of CO_2 formation via primary pathways ($CO* + O* \rightarrow CO_2 + 2*$; step 10 in Scheme 1), are similar for H_2/CO and D_2/CO reactants

19764 *J. Phys. Chem. C, Vol. 114, No. 46, 2010*

Ojeda et al.

(0.46 and 0.48 mol h^{-1} g-at Fe^{1-}, respectively). This is consistent with the formation of O* species in elementary steps that do not involve hydrogen-derived species, as is the case for unassisted CO dissociation pathways.

The assumptions of pseudo steady-state for all adsorbed species in Scheme 1, quasi-equilibrium for reactants adsorption and formyl species formation (steps 1−3), and CO* coverages at near saturation values, give an equation for hydrocarbon synthesis rates as the combined rates of H-assisted and unassisted pathways:

$$r_{HC}^{overall} = r_{HC}^{assisted} + r_{HC}^{unassisted} = \frac{K_1 K_2 K_3 k_4 P_{CO} P_{H_2}}{(1 + K_1 P_{CO})^2} +$$

$$\frac{K_1 k_6 P_{CO}}{(1 + K_1 P_{CO})^2} \quad (1)$$

where k_i and K_i are the rate and equilibrium constants for the ith step in Scheme 1, respectively. Our previously reported rate data[10] show that both terms, and their respective sequences, contribute to measured rates on Fe-based catalysts. The first and second terms accurately describe measured rates of formation of H_2O and CO_2, respectively, indicating that CO_2 forms exclusively via scavenging of O* species formed only via unassisted CO dissociation,[32] while H_2O forms only via OH* groups formed in H-assisted dissociation. The H-assisted CO dissociation route is the predominant pathway on the Fe-based catalysts at the low-temperature and high pressure conditions that lead to the preferential formation of the desired C_{5+} FTS products.[10]

The second term in eq 1 does not contain any terms that are sensitive to H_2 or D_2, because it depends only on the equilibrium adsorption constant (K_1) and the unassisted dissociation rate constant (k_6) for CO:

$$r_{HC}^{unassisted} = \frac{K_1 k_6 P_{CO}}{(1 + K_1 P_{CO})^2} \quad (2)$$

This is consistent with the rate data in Figure 1, which show no H_2/D_2 isotope effect for primary CO_2 formation pathways. Measured kinetic isotope effects reflect, therefore, the influence of H_2/CO and D_2/CO reactants on hydrocarbon formation rates via the hydrogen-assisted CO dissociation pathways given by the first term in eq 1:

$$r_{HC}^{assisted} = \frac{K_1 K_2 K_3 k_4 P_{CO} P_{H_2}}{(1 + K_1 P_{CO})^2} \quad (3)$$

These rates with H_2/CO and D_2/CO reactants are obtained from:

$$r_{HC}^{assisted} = r_{HC}^{overall} - r_{HC}^{unassisted} \quad (4)$$

where the rate of hydrocarbon synthesis via the unassisted route equals the rate of primary CO_2 formation (eq 2; 0.46 and 0.48 mol h^{-1} g-at Fe^{1-} for H_2/CO and D_2/CO, respectively) because CO_2 is formed via scavenging of O* species exclusively originating from direct CO* dissociation steps.

The ratio of the rates of hydrocarbon formation via hydrogen-assisted pathways with H_2/CO (r_H) and D_2/CO (r_D) reactants is
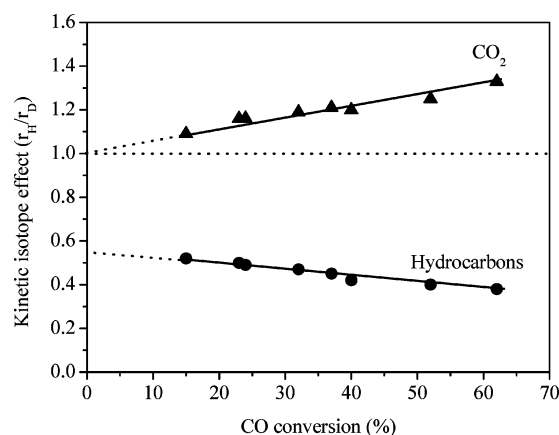
Figure 2. Kinetic isotope effect for hydrocarbon formation via H-assisted CO dissociation and CO_2 formation rate as a function of CO conversion with H_2/CO or D_2/CO over Fe−Zn−K−Cu catalyst (Zn/Fe = 0.1, K/Fe = 0.02, Cu/Fe = 0.01) at 508 K and 2.14 MPa.

shown in Figure 2 as a function of CO conversion. Isotope effects led to different CO conversion levels with H_2/CO and D_2/CO; as a result, calculated r_H values were estimated by interpolation to match the conversion level at each measured r_D value. A similar interpolation procedure was used to obtain r_D at the conversion level for each measured r_H value. These ratios decreased from 0.49 to 0.29 as CO conversion increased from 15% to 62%, possibly as a result of different inhibition effects by H_2O and D_2O on reaction rates. The value of the isotope effect by extrapolation of the data in Figure 2 to zero conversion (0.56) reflects the ratio of rates in the absence of water inhibition effects; this value is used in mechanistic interpretations of these H_2/D_2 isotope effects.

The effects of isotopic identity on the rate of hydrogen-assisted CO dissociation rates (the first term in eq 1) depend on K_2, K_3, and k_4 according to:

$$KIE = \frac{r_H}{r_D} = \frac{K_2^H K_3^H k_4^H}{K_2^D K_3^D k_4^D} = \frac{K_2^H}{K_2^D} \cdot \frac{K_3^H}{K_3^D} \cdot \frac{k_4^H}{k_4^D} \quad (5)$$

where r_H and r_D represent hydrocarbon synthesis rates via hydrogen-assisted pathways with H_2/CO and D_2/CO, respectively, and all superscripts denote the hydrogen isotope. All other terms ($K_1^H; K_1^D$) cancel because neither hydrogen nor hydrogen-derived intermediates are involved in the corresponding elementary steps. These KIE values reflect a combination of thermodynamic (K_2 and K_3) and kinetic (k_4) effects of isotopic identity. In what follows, we report DFT calculations on CO-saturated Fe(110) model surfaces to probe the origins of these H_2/D_2 isotope effects for FTS reactions via H-assisted CO dissociation kinetically relevant steps.

3.2. Theoretical Analysis of H_2/D_2 Isotope Effects on H-Assisted CO Dissociation Pathways on CO-Saturated Fe(110) Model Surfaces. Isotope effects reflect differences in rate and equilibrium constants for elementary steps involving deuterium and hydrogen isotopomers of specific intermediates. Differences in rate constants reflect corresponding differences in the zero-point energy (ZPE)-corrected activation energy barriers (E) and in the pre-exponential factors (A) as a result of entropy differences (ΔS) between H and D isotopomers. Both ZPE and entropy values can be calculated from vibrational frequencies (v_i) of relevant stable species and transition states. The relevant formulas are presented in the Appendix. As

H$_2$/D$_2$ Isotope Effects in FTS on Fe and Co Catalysts

J. Phys. Chem. C, Vol. 114, No. 46, 2010 **19765**

TABLE 1: DFT-Calculated Kinetic (KIE) and Equilibrium (IE) Isotope Effects of Elementary Steps on CO-Saturated Fe(110) Model Surfaces

Entry	Elementary step or sequence	ZPE contribution	Entropic contribution	Overall KIE or IE
1	H$_2$ + 2* $\rightleftarrows$ 2H*	0.37	1.65	0.62
2	CO* + H* $\rightleftarrows$ HCO* + *	0.74	1.06	0.78
3	HCO* + H* → HCOH* + *	0.74	1.11	0.82
4	H$_2$/CO → HCO* → HCOH*			0.40

discussed in the Methods section (2.3), DFT allows estimates of vibrational frequencies for the initial, transition, and final states involved in each elementary step, as well as isotope effect estimates from first principles.

Classically, the substitution of a H-atom with a heavier D-atom decreases the vibrational frequencies for any chemical bond containing D and the respective ZPE values. When the D isotope is present in the chemical bond being broken or formed along the reaction coordinate, primary KIE leads, respectively, to lower or higher rates for deuterated species, respectively. Our calculations indicate, however, that the origins of these isotope effects are more complex and that the details of entropic contributions to isotope effects need to be rigorously considered. Accurate estimates of isotope effects require that we rigorously consider the contributions from activation barriers (henceforth denoted by Ω_H/Ω_D), and from pre-exponential factors (henceforth denoted by A_H/A_D). These isotope effects can then be expressed as the product of two terms:

$$\frac{k_H}{k_D} = \frac{A_H}{A_D} \cdot \frac{\Omega_H}{\Omega_D} \qquad (6)$$

Additional details related to the derivation of these formulas are provided in the Appendix.

In addition, the frequency of the main bond-breaking mode is not only the one affected by isotopic substitution. The frequencies (and ZPE values) of the D-containing intermediates are smaller not only in the initial reactant state (IS), but also in the transition state (TS). It is the difference in isotope effects between reactants and transition states in an elementary step [{ZPE$_D^{TS}$ − ZPE$_D^{IS}$} versus {ZPE$_H^{TS}$ − ZPE$_H^{IS}$}] that determines the Ω_H/Ω_D term. Typically, the mechanistic interpretation of isotope effects focuses on the chemical bond being formed or broken; we find, however, that chemical bonds that remain unchanged as reactants convert to products contribute significantly to the Ω_H/Ω_D and A_H/A_D terms that define measured k_H/k_D terms.

In a species such as HCOH*, hydrogen substitution effects by deuterium are twofold. The rate constant for the step that forms HCOH* (HCO* + H* → HCOH* + *) is affected by the isotopic identity of the H*/D* atom added to HCO* (primary isotope effect), but also because of the different isotope in HCO*/DCO* (secondary isotope effect).

ZPE and entropy contributions to isotope effects in FTS reactions on CO-saturated Fe(110) model surfaces are shown in Table 1. The combination of the isotope effects for all steps involved in H-assisted CO dissociation (0.62 for H$_2$ dissociation (step 2, Scheme 1), 0.78 for HCO* formation (step 3, Scheme 1), and 0.82 for HCOH* formation (step 4, Scheme 1)) gives a product of 0.40 for the overall isotope effect (r_H/r_D). As shown in section 3.1, the value extrapolated to zero CO conversion from measured rates is 0.56. Thus, the calculated KIE value

SCHEME 2: Chain Growth and Termination Reactions in Fischer−Tropsch Synthesis with Fe Catalysts
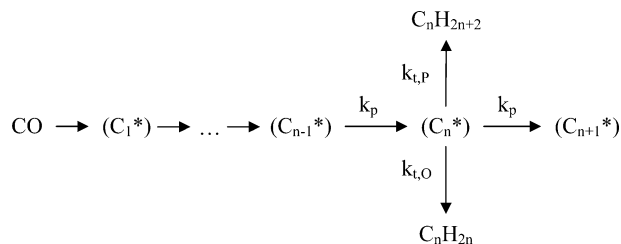
(0.40) at 0.5 CO* monolayer on Fe model surfaces is in reasonable agreement with measured values. We note that the rate and equilibrium constants that appear in the overall rate equation correspond to three elementary steps that individually exhibit inverse isotope effects, including a strong inverse effect for the equilibrium isotope effect for H$_2$ dissociation (0.62).

The differences between calculated (0.40) and measured (0.56) isotope effects may reflect calculations performed on model surfaces at coverages that cannot be directly related to the fully saturated surfaces present during FTS catalysis. In addition, the accuracy of the second-derivative methods and numerical procedures required to estimate vibrational frequencies may exacerbate errors when these values are used to estimate isotope effects. In particular, the equilibrium and kinetic isotope effects (see Appendix) depend exponentially on ZPE and entropy values, making the resulting overall isotope effects very sensitive to small inaccuracies in DFT-based frequency estimates. Nevertheless, the agreement between theory and data confirms the inverse nature of the isotope effects involved and the predominant involvement of H-assisted CO dissociation steps instead of unassisted pathways that would have led to reaction rates independent of isotopic identity.

3.3. H$_2$/D$_2$ Isotope Effects on Reaction Selectivity. FTS selectivities depend on the rates of propagation of alkyl chains via stepwise addition of monomers formed via assisted or unassisted CO dissociation steps.[33] These chains terminate via hydrogen addition or elimination to form paraffins or olefins, respectively (Scheme 2). Carbon number selectivities depend on the relative rates of propagation ($r_{p,n}$) and termination ($r_{t,n}$) of chains with n-carbons. The chain termination probability (β_n) can be determined from the rates of formation of individual products with n-carbons using:

$$\beta_n = \phi_n / \sum_{i=n+1}^{\infty} \phi_i = \frac{r_{t,n}}{r_{p,n}} \qquad (7)$$

where ϕ_n is the mole fraction of a given hydrocarbon among products. The β_n values reported here were estimated by assuming that the chain growth probability (α) calculated for C$_4$−C$_9$ chains from Anderson−Schulz−Flory plots remains constant for larger chains. The mole fraction for these larger chains is then given by:

$$\phi_n = \alpha \cdot \phi_{n-1} \qquad (8)$$

These mole fractions were then used to obtain β_n values for all chains using eq 7. We have found that chain termination probabilities for C$_1$−C$_{13}$ hydrocarbons are similar with H$_2$/CO or D$_2$/CO reactants (Figure 3) and lead to similar product distributions for a given CO conversion level (Table 2). Chain termination probabilities decreased with increasing carbon
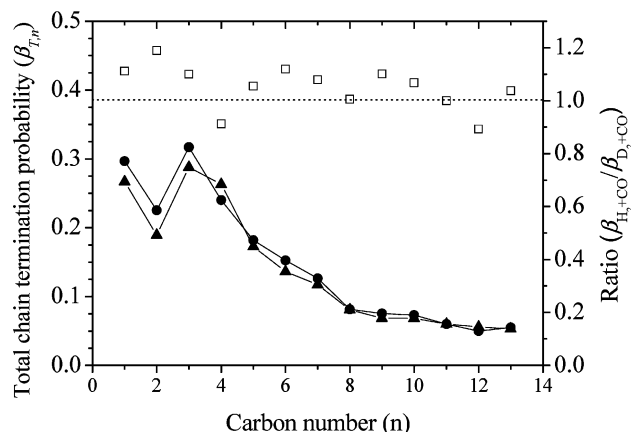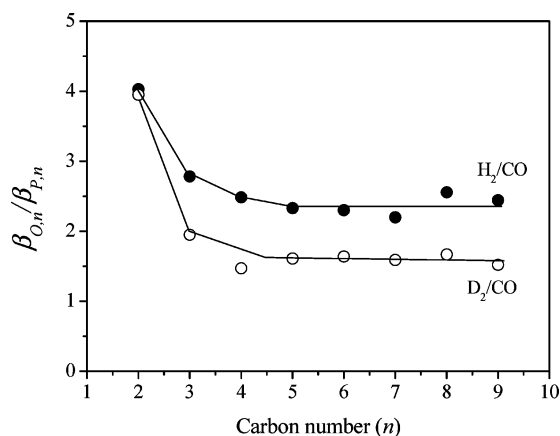
Figure 3. Total and ratio (□) of total chain termination probabilities for C_1–C_{13} hydrocarbons with H_2/CO (●) or D_2/CO (▲) at ~22% CO conversion over Fe–Zn–K–Cu catalyst (Zn/Fe = 0.1, K/Fe = 0.02, Cu/Fe = 0.01) at 508 K and 2.14 MPa.

TABLE 2: Product Distribution Obtained with H_2/CO or D_2/CO over Fe–Zn–K–Cu Catalyst (Zn/Fe = 0.1, K/Fe = 0.02, Cu/Fe = 0.01) at 508 K and 2.14 MPa

	space velocity (mol$_{CO}$ h^{-1} g$_{Fe}^{-1}$)	CO conv. (%)	selectivity (%, carbon basis)[a]			
			CO_2	C_1	C_2–C_4	C_{5+}
H_2/CO	0.29	23.6	25.0	2.8	13.6	83.6
D_2/CO	0.49	22.6	13.6	1.9	12.7	85.4

[a] Hydrocarbon selectivities are reported CO_2-free.

Figure 4. Ratio of termination probabilities as olefins ($\beta_{O,n}$) or paraffins ($\beta_{P,n}$) with H_2/CO or D_2/CO at ~22% CO conversion over Fe–Zn–K–Cu catalyst (Zn/Fe = 0.1, K/Fe = 0.02, Cu/Fe = 0.01) at 508 K and 2.14 MPa.

number and approached an asymptotic value of 0.055 for C_{10+} hydrocarbons for both H_2/CO and D_2/CO.

The total termination probability combines the rates of termination pathways to olefins ($\beta_{O,n}$) and paraffins ($\beta_{P,n}$) via H-abstraction and H-addition, respectively:

$$\beta_{T,n} = \beta_{O,n} + \beta_{P,n} \qquad (9)$$

The ratio of termination rates as olefins and paraffins ($\beta_{O,n}/\beta_{P,n}$) is smaller for D_2/CO than for H_2/CO reactants (Figure 4). In the context of Scheme 2, these termination probability ratios are given by:

$$\beta_{O,n} = \frac{k_{t,O}[C_n^*]}{k_p[CH_x^*][C_n^*]} = \frac{k_{t,O}}{k_p[CH_x^*]} \qquad (10)$$

$$\beta_{P,n} = \frac{k_{t,P}[H^*][C_n^*]}{k_p[CH_x^*][C_n^*]} = \frac{k_{t,P}[H^*]}{k_p[CH_x^*]} \qquad (11)$$

Therefore, the ratio of termination rates as olefins and paraffins ($\beta_{O,n}/\beta_{P,n}$) can be written as:

$$\frac{\beta_{O,n}}{\beta_{P,n}} = \frac{k_{t,O}}{k_{t,P}} \cdot \frac{1}{[H^*]} \qquad (12)$$

Equation 12 indicates that for a specific chain size, the olefin content would increase with increasing $k_{t,O}/k_{t,P}$ ratios and decrease with increasing hydrogen (or deuterium) coverage. The relative value of the $\beta_{O,n}/\beta_{P,n}$ ratio ($n > 3$) for D_2/CO with respect to H_2/CO reactants is 0.68, which is similar to the theoretically calculated value for the equilibrium isotope effect on H_2 dissociation ($K_2^H/K_2^D = 0.62$), indicating that isotope effects on $k_{t,O}/k_{t,P}$ ratios are near unity and that H-abstraction and H-addition rate constants have similar KIE values. Indeed, olefin formation involves the cleavage of carbon–hydrogen chemical bonds and the creation of metal–hydrogen bonds, while paraffin formation requires instead the making and breaking of the same carbon–hydrogen and metal–hydrogen bonds, respectively. Thus, we expect that KIE for olefin and paraffin formation would nearly compensate, especially if the transition state is located approximately halfway along the reaction coordinate. Therefore, we conclude that the lower olefin/paraffin ratio observed with D_2/CO instead of H_2/CO merely reflects a higher D* surface coverage (as compared to that of H*).

3.4. Comparison of H_2/D_2 Isotope Effects on Fe and Co FTS Catalysts. Experimental H_2/D_2 isotope effects have been previously reported on Co at FTS conditions leading to high chain growth probabilities,[18] and the inverse KIE values measured ($r_H/r_D = 0.80$; Co/SiO$_2$, 473 K, 2 MPa, $H_2(D_2)$/CO = 2) were interpreted as thermodynamic effects due to the relative magnitude of H_2 and D_2 adsorption equilibrium constants. These conclusions are consistent with the lower olefin/paraffin ratios measured with D_2/CO reactants, but not with the similar chain growth probabilities measured for C_1–C_{12} hydrocarbons with H_2/CO and D_2/CO. Interestingly, similar H_2/D_2 effects on hydrocarbon formation rates, olefin/paraffin ratio, and chain growth probability are found here for Fe-based catalysts.

Recent experimental and theoretical studies have shown that CO dissociation occurs on Co-based catalysts predominantly via H-assisted routes (steps 1–5, 8, 9 in Scheme 1).[10] On model CO-saturated Co(0001) surfaces, these routes specifically involve HCO* and HCOH* intermediates, similar to those proposed for H-assisted CO dissociation routes on CO-saturated Fe(110) surfaces. On Co, the potential energy surfaces indicate that alternate paths involving sequential H-addition to form COH* and HCOH* also contribute to CO dissociation rates. The assumptions of pseudo steady-state for all adsorbed species, quasi-equilibrium for steps 1–3 (Scheme 1), and CO* coverages at near saturation values give the following equation for hydrocarbon synthesis rates on Co-based FTS catalysts:

H$_2$/D$_2$ Isotope Effects in FTS on Fe and Co Catalysts

J. Phys. Chem. C, Vol. 114, No. 46, 2010 **19767**

$$r_{HC} = r_{HC}^{assisted} = \frac{K_1 K_2 K_3 k_4 P_{CO} P_{H_2}}{(1 + K_1 P_{CO})^2} \qquad (13)$$

As on Fe, rate data on Co-based catalysts indicate that the first H-addition to CO* step (to form HCO* and/or COH*) is quasi-equilibrated, making the second H-addition the sole kinetically relevant step. The effects of isotopic identity on hydrocarbon formation rates depend on K_2, K_3, and k_4 as also found on Fe-based catalysts.

Next, we report DFT-derived rate and equilibrium constants for the various elementary steps involved in CO reactions with H$_2$ or D$_2$ on Co(0001) surfaces saturated with CO* using the same steps and procedures used for CO-saturated Fe(110) surfaces. The calculated thermodynamic and kinetic isotope effects for the two possible routes (HCO* or COH* intermediates) on CO-saturated Co(0001) model surfaces are shown in Table 3. The DFT-derived values for r_H/r_D are 0.70 and 0.49, depending on whether CO dissociation proceeds via HCO* or COH*, respectively. The experimentally measured KIE value[18] (0.80) is similar to that derived for HCO* intermediates,[18] suggesting that HCO*-mediated steps prevail on Co-based catalysts at conditions leading to significant chain growth, as also found on Fe-based catalysts.[10] Thus, on both surfaces, CO dissociation is assisted by chemisorbed hydrogen and proceeds via the quasi-equilibrated formation of formyl species (HCO*) that undergo subsequent hydrogenation to HCOH* in the kinetically relevant step.

A comparison of the three elementary steps that contribute to the overall isotope effects on Co and Fe surfaces indicates that: (i) H$_2$ dissociation on CO-saturated Co(0001) and Fe(110) surfaces gives similar inverse thermodynamic isotope effects (0.61 and 0.62, respectively); (ii) the formation of HCO* species on Co(0001) and Fe(110) gives inverse thermodynamic isotope effects of 0.64 and 0.78, respectively; and (iii) HCOH* formation gives very different kinetic isotope effects on Co(0001) and Fe(110) (1.79 and 0.82, respectively). Both Co and Fe model surfaces give inverse overall KIE values, but the very different isotope effects for the second H-addition step (1.79 and 0.82) lead to smaller overall isotope effects on Co than on Fe (0.70 and 0.40, respectively), in agreement with similar differences obtained from experimental rate data (0.80 and 0.56 for Co and Fe catalysts, respectively). Our calculations indicate that these large differences in the kinetic isotope effects for H-addition to HCO* on Co and Fe reflect concomitant differences in the differential ZPE values (for HCO*, H*, and the transition state to HCOH* formation), which are notably different on the two surfaces: the ZPE contribution to the KIE

for that step is 0.74 on Fe, whereas on Co this contribution is 1.61 (see Tables 1 and 3). Quantitative details of the vibrational modes used in these calculations are included in the Supporting Information.

Identifying the source of the discrepancy in the ZPE correction of the barrier for the HCOH* formation step on the two metals is far from trivial, given the contributions by more than 20 vibrational modes accounted for in the ZPE calculations (see the Supporting Information). However, one can suggest that because the higher frequency modes are contributing the most to the ZPE correction of the initial state (IS) and the transition state (TS), some chemical rationalization of that difference might be possible. Because the analysis is similar for the H-containing isotopes (H* + HCO* → HCOH*) and the D-containing isotopes (D* + DCO* → DCOD*), the difference stemming from a mass-scaling factor between the two, we only refer our analysis below to the H-containing isotopes. In particular, by focusing on the highest frequency mode of the TS and the IS, we observe that for the H-containing species on Fe, the largest frequency for the IS is 3023 cm^{-1} (C−H stretch in HCO*), whereas for the TS the largest frequency is 3076 cm^{-1} (C−H stretch in H−C−O−H†). In contrast, for the H-containing species on Co, the highest vibrational frequency is again for the C−H stretch mode in HCO*, which is 2558 cm^{-1}, whereas for the TS the largest frequency is 2999 cm^{-1} (C−H stretch in H−C−O−H†). We note that the C−H stretch mode is not along the reaction coordinate responsible for making the O−H bond in HCOH*, which is the product of this elementary step, but rather the vibrational frequency of a secondary, spectator bond (C−H). These data suggest that the highest frequency mode is mostly preserved along the reaction coordinate of HCO* + H* → HCOH* + * (from IS to TS) on Fe, whereas there is a substantial increase in the highest frequency for the TS on Co (as compared to the highest frequency of the IS on Co). On Fe, the difference between the highest frequency of IS and TS is only 53 cm^{-1}, whereas that difference is 441 cm^{-1} on Co, which leads to the much more substantial ZPE correction and KIE on cobalt than on iron.

3.5. Thermodynamic Isotope Effect for H$_2$/D$_2$ Dissociation. Given the commonality of H$_2$ dissociation in many processes catalyzed by transition metals, and the lack of available data on possible isotope effects on this process, we now turn our attention to the results of our theoretical analysis for that effect. On both Fe(110) and Co(0001) surfaces, H$_2$/D$_2$ dissociation was studied in the presence of 0.5 ML CO coverage, and we only consider the thermodynamic isotope effect, because H$_2$/D$_2$ dissociation are quasi-equilibrated during most hydrogenation reactions (see Scheme 1). We do not find any adsorbed molecular H$_2$ precursors; therefore, we take H$_2$(g) as the reference initial state for dissociation processes. Table 4 provides detailed data on the individual contributions to the overall thermodynamic isotope effect for this process. Interestingly, the ZPE and entropy corrections to the initial and final state energies on both Fe and Co surfaces are, within the accuracy of our methods, identical to each other for each of the relevant individual terms. Apparently, the interaction of atomic H (that is the only important factor here, as the initial state is gas phase H$_2$) with the CO-saturated Co and Fe surfaces is fairly weak and rather insensitive to the nature of the metal. As a result, the isotope effect calculated for the two surfaces is practically the same in terms of both its energy and entropy components. In particular, entropy alone would favor H$_2$ over D$_2$ dissociation at the conditions of our experiments by a factor of ca. 1.65 (normal isotope effect), whereas energy alone would favor D$_2$

TABLE 3: DFT-Calculated Kinetic (KIE) and Equilibrium (IE) Isotope Effects of Elementary Steps on CO-Saturated Co(0001) Model Surfaces

Entry	Elementary step or sequence	ZPE contribution	Entropic contribution	Overall KIE or IE
1	H$_2$ + 2* ⇌ 2H*	0.37	1.66	0.61
2	CO* + H* ⇌ HCO* + *	0.59	1.08	0.64
3	HCO* + H* → HCOH* + *	1.61	1.11	1.79
4	H$_2$/CO → HCO* → HCOH*			0.70
5	CO* + H* ⇌ COH* + *	0.63	1.03	0.66
6	COH* + H* → HCOH* + *	1.07	1.16	1.24
7	H$_2$/CO → COH* → HCOH*			0.49

19768 *J. Phys. Chem. C, Vol. 114, No. 46, 2010*

Ojeda et al.

TABLE 4: Vibrational Frequencies, Entropies, ZPE Corrections, and Details of Thermodynamic Isotope Effect Calculations for H_2 and D_2 Dissociative Adsorption on CO-Saturated Fe(110) and Co(0001) Surfaces[a]

	CO-saturated Fe(110)		CO-saturated Co(0001)	
	H	D	H	D
ν_{IS} (cm^{-1})	4430	3134	4430	3134
ν_{FS} (cm^{-1})	1303	921	1271	899
	1150	813	1209	855
	1150	813	1171	828
	1141	807	1085	768
	1107	783	1074	760
	938	663	1031	729
S_{IS} (J mol^{-1} K^{-1})	150.7	164.5	150.7	164.5
S_{FS} (J mol^{-1} K^{-1})	9.0	18.8	8.8	18.4
A_H/A_D	1.65		1.66	
ZPE$_{IS}$ (kJ mol^{-1})	26.5	18.8	26.5	18.8
ZPE$_{FS}$ (kJ mol^{-1})	40.7	28.8	40.9	28.9
Ω_H/Ω_D	0.37		0.37	
overall isotope effect	0.62		0.61	

[a] IS: initial state (H_2 or D_2 in gas phase). FS: final state (adsorbed H or D atoms on model surfaces).

over H_2 dissociation (inverse isotope effect of 0.37). The product of the two terms leads to an overall inverse thermodynamic isotope effect for the equilibrated H_2/D_2 dissociation of ca. 0.61, favoring D_2 dissociation over H_2 dissociation.

3.6. H_2/D_2 Isotope Effect on CO_2 Formation via Secondary Pathways. CO_2 formation rates via secondary pathways, involving H_2O readsorption and dissociation to give O* species, which are subsequently removed via reaction with CO*, also differ for D_2/CO and H_2/CO reactants (Figure 1B). CO_2 formation rates increase as conversion increases with increasing residence time, and the corresponding slope reflects the synthesis of CO_2 by reaction of water-derived O* species with CO ($CO + H_2O \rightarrow CO_2 + H_2$). Figure 2 shows an increasing normal kinetic isotope effect ($r_H/r_D > 1$) for CO_2 formation rates via secondary pathways as CO conversion levels increase. This implies that the extent of H_2O readsorption on active sites to eventually form O* that can be removed as CO (reverse step 9 in Scheme 1 and subsequent OH* dissociation) is more significant when compared to that of D_2O species. The higher relative readsorption of H_2O species is also evidenced by the decrease of KIE values for hydrocarbon formation as CO conversion (and the concomitant water concentration) increases (Figure 2; section 3.1). Therefore, our data suggest that the energy required for O* to be formed from D_2O (cleavage of O–D bonds) is higher than that needed from H_2O, and that this difference is higher than that resulting of the stronger surface-D bonds (as compared to surface-H bonds).

4. Conclusions

The observed H/D kinetic isotope effect during FTS with Fe and Co catalysts is the result of the combination of thermodynamic (hydrogen adsorption and first H-addition to CO* species) and kinetic (second H-addition) isotope effects in hydrocarbon formation via H-assisted CO dissociation pathways. The inverse equilibrium isotope effect corresponding to H_2/D_2 adsorption results also in lower probabilities of chain termination steps as olefins instead of paraffins. Primary formation of CO_2, which involves scavenging of O* atoms formed via direct CO dissociation by coadsorbed CO, shows no H_2/D_2 isotope effect. In contrast, CO_2 formation via secondary water–gas shift pathways shows inverse isotope effects. These results are consistent with a FTS mechanism involving parallel H-assisted and unassisted CO dissociation leading

to H_2O and CO_2, respectively, as the oxygen rejection products. Consistent with experiments, DFT-calculated results indicate an inverse KIE for both Fe and Co surfaces, with specific calculated values fairly close to experimentally determined ones.

Supporting Information Available: Vibrational frequencies for adsorbed species on CO-saturated Fe(110) and Co(0001) model surfaces. Tables with key bond lengths and angles in relevant FTS intermediates. Tables with the effect of coadsorbed CO on the vibrational frequencies of key reaction intermediates. Images showing the geometry of adsorbed species and the initial, transition, and final states for selected elementary steps on Fe(110) and Co(0001) in the presence of 0.5 ML of coadsorbed CO. This material is available free of charge via the Internet at http://pubs.acs.org.

Appendix

ZPE Correction

$$\text{ZPE} = \frac{hc}{2} \sum_i^{\text{no. of modes}} \frac{1}{\lambda_i}$$

$$E_f = E_f^{\text{uncorrected}} + \text{ZPE}^{\text{TS}} - \text{ZPE}^{\text{IS}}$$
$$\Delta E = \Delta E^{\text{uncorrected}} + \text{ZPE}^{\text{FS}} - \text{ZPE}^{\text{IS}}$$

Vibrational Entropy Calculation

$$S_{\text{vib}} = R \sum_i^{\text{no. of modes}} \left(\frac{x_i}{e^{x_i} - 1} - \ln(1 - e^{-x_i}) \right)$$

where

$$x_i = \frac{hc}{k_B T} \frac{1}{\lambda_i}$$

H₂/D₂ Isotope Effects in FTS on Fe and Co Catalysts

J. Phys. Chem. C, Vol. 114, No. 46, 2010 **19769**

3D Translational Contribution to Entropy (Gas-Phase Molecules)

$$S_{\text{trans}}^{\text{3D}} = R\left\{\log\left[\frac{2\pi m k_B T}{h^2}\right]^{3/2}\frac{k_B T}{P} + 2.5\right\}$$

Rotational Contribution to Entropy (Gas-Phase Molecules, Linear Case)

$$S_{\text{rot}} = R\left\{\log\left[\frac{8\pi^2 I_{\text{max}} k_B T}{s_{\text{number}} h^2}\right] + 1.5\right\}$$

Reaction Rate

$$r_{AB} = \frac{k_B T}{h}\exp\left(\frac{\Delta S^{\text{OTS}-\text{IS}}}{R}\right)\exp\left(-\frac{\Delta H^{\text{OTS}-\text{IS}}}{k_B T}\right)n_A n_B$$

Note that the ΔH term calculated from DFT is approximated by ΔE.

Equilibrium Constant

$$K_{\text{eq}} = \exp\left\{\left(\frac{-1}{RT}\right)(\Delta H^{\text{FS}-\text{IS}} - T\Delta S^{\text{FS}-\text{IS}})\right\}$$

Kinetic Isotope Effect (KIE)

$$\frac{k_H}{k_D} = \frac{A_H}{A_D}\frac{\Omega_H}{\Omega_D}$$

ZPE Contribution to KIE (H/D)

$$\frac{\Omega_H}{\Omega_D} = \exp\left((-1)\frac{(\text{ZPE}_H^{\text{TS}} - \text{ZPE}_H^{\text{IS}}) - (\text{ZPE}_D^{\text{TS}} - \text{ZPE}_D^{\text{IS}})}{k_B T}\right)$$

Entropic Contribution to KIE (H/D) (Pre-exponential Factor)

$$\frac{A_H}{A_D} = \exp\left(\frac{(S_H^{\text{TS}} - S_H^{\text{IS}}) - (S_D^{\text{TS}} - S_D^{\text{IS}})}{R}\right)$$

Note that the actual barrier does not appear in this expression, only the ZPE corrections.

Pre-exponential also has the term $k_B T/h$, but this is neglected because it does not change for H and D.

The coverage term ($n_A n_B$) is assumed to be identical for H and D.

Equilibrium Isotope Effect (IE)

$$\frac{K_{\text{eq}}^H}{K_{\text{eq}}^D} = \exp\left\{\left(\frac{-1}{RT}\right)[\Delta H^H - \Delta H^D]\right\}\cdot\exp\left\{\left(\frac{1}{R}\right)[\Delta S^H - \Delta S^D]\right\}$$

$$\frac{K_{\text{eq}}^H}{K_{\text{eq}}^D} = \left[\frac{K_{\text{eq}}^H}{K_{\text{eq}}^D}\right]^{\text{ZPE}}\cdot\left[\frac{K_{\text{eq}}^H}{K_{\text{eq}}^D}\right]^{\text{entropy}}$$

ZPE Contribution to IE (H/D)

$$\left[\frac{K_{\text{eq}}^H}{K_{\text{eq}}^D}\right]^{\text{ZPE}} = \exp\left((-1)\frac{(\text{ZPE}_H^{\text{FS}} - \text{ZPE}_H^{\text{IS}}) - (\text{ZPE}_D^{\text{FS}} - \text{ZPE}_D^{\text{IS}})}{k_B T}\right)$$

Entropic Contribution to IE (H/D)[34]

$$\left[\frac{K_{\text{eq}}^H}{K_{\text{eq}}^D}\right]^{\text{entropy}} = \exp\left(\frac{(S_H^{\text{FS}} - S_H^{\text{IS}}) - (S_D^{\text{FS}} - S_D^{\text{IS}})}{R}\right)$$

Legend

h	Planck's constant
c	speed of light
$(1)/(\lambda_i)$	wavenumber corresponding to each vibrational frequency
E_f	ZPE-corrected activation energy (forward)
ZPE	zero-point energy
ΔE	reaction energy
S_{vib}	vibrational entropy
R	ideal gas constant
k_B	Boltzmann constant
m	molecular mass
T	reaction temperature
P	reaction pressure
I_{max}	principal moment of inertia
s_{number}	symmetry number for the molecule (2 for H₂)
r_{AB}	reaction rate
K_{eq}	equilibrium constant
Ω_H, Ω_D	rate constant without pre-exponential contribution
$[(K_{\text{eq}}^H)/(K_{\text{eq}}^D)]^{\text{ZPE}}$	ZPE contribution to equilibrium isotope effect
$[(K_{\text{eq}}^H)/(K_{\text{eq}}^D)]^{\text{entropy}}$	entropic contribution to equilibrium isotope effect
$(\Omega_H)/(\Omega_D)$	ZPE contribution to kinetic isotope effect
$(A_H)/(A_D)$	entropic contribution to kinetic isotope effect

References and Notes

(1) Khodakov, A. Y.; Chu, W.; Fongarland, P. *Chem. Rev.* **2007**, *107*, 1692–1744.

(2) van Steen, E.; Claeys, M. *Chem. Eng. Technol.* **2008**, *31*, 655–666.

(3) Li, S.; Li, A.; Krishnamoorthy, S.; Iglesia, E. *Catal. Lett.* **2001**, *77*, 197–205.

(4) Fischer, F.; Tropsch, H. *Brenntoff-Chem.* **1926**, *7*, 97–116.

(5) Wojciechowski, B. W. *Catal. Rev.-Sci. Eng.* **1988**, *30*, 629–702.

(6) Eliason, S. A.; Bartholomew, C. H. *Appl. Catal., A* **1999**, *186*, 229–243.

(7) Adesina, A. A. *Appl. Catal., A* **1996**, *138*, 345–367.

(8) Wang, Y. N.; Ma, W. P.; Lu, Y. J.; Yang, J.; Xu, Y. Y.; Xiang, H. W.; Li, Y. W.; Zhao, Y. L.; Zhang, B. J. *Fuel* **2003**, *82*, 195–213.

(9) van der Laan, G. P.; Beenackers, A. A. C. M. *Appl. Catal., A* **2000**, *193*, 39–53.

(10) Ojeda, M.; Nabar, R.; Nilekar, A. U.; Ishikawa, A.; Mavrikakis, M.; Iglesia, E. *J. Catal.* **2010**, *272*, 287–297.

(11) Dalla Betta, R. A.; Shelef, M. *J. Catal.* **1977**, *49*, 383–385.

(12) Shelef, M.; Dalla Betta, R. A. *J. Catal.* **1979**, *60*, 169–170.

(13) Wilson, T. P. *J. Catal.* **1979**, *60*, 167–168.

Ojeda et al.

(14) van Nisselrooij, P. F. M. T.; Luttikholt, J. A. M.; van Meerten, R. Z. C.; de Croon, M. H. J. M.; Coenen, J. W. E. *Appl. Catal.* **1983**, *6*, 271–281.

(15) McKee, E. W. *J. Catal.* **1967**, *8*, 240–249.

(16) Kellner, C. S.; Bell, A. T. *J. Catal.* **1981**, *67*, 175–185.

(17) Costa, J. L.; Noels, A. F.; Demonceau, A.; Hubert, A. J. *J. Catal.* **1987**, *105*, 1–9.

(18) Krishnamoorthy, S.; Tu, M.; Ojeda, M. P.; Pinna, D.; Iglesia, E. *J. Catal.* **2002**, *211*, 422–433.

(19) Li, S.; Krishnamoorthy, S.; Li, A.; Meitzner, G. D.; Iglesia, E. *J. Catal.* **2002**, *206*, 202–217.

(20) Davis, B. H. Technology development for iron and cobalt Fischer−Tropsch catalysts. Report Number FC26-98FT40308, OSTI ID 806693, Department of Energy, U.S., 2002.

(21) Raje, A. P.; O'Brien, R.; Davis, B. H. *J. Catal.* **1998**, *180*, 36–43.

(22) van der Laan, G. P.; Beenackers, A. A. C. M. *Ind. Eng. Chem. Res.* **1999**, *38*, 1277–1290.

(23) Hammer, B.; Hansen, L. B.; Nørskov, J. K. *Phys. Rev. B* **1999**, *59*, 7413–7421.

(24) Greeley, J.; Nørskov, J. K.; Mavrikakis, M. *Annu. Rev. Phys. Chem.* **2002**, *53*, 319–348.

(25) Borthwick, D.; Fiorin, V.; Jenkins, S. J.; King, D. A. *Surf. Sci.* **2008**, *602*, 2325.

(26) Shetty, S.; Jansen, A. P. J.; van Santen, R. A. *J. Am. Chem. Soc.* **2009**, *131*, 12874.

(27) Sorescu, D. C. *J. Phys. Chem. C* **2008**, *112*, 10472.

(28) Sorescu, D. C. *J. Phys. Chem. C* **2009**, *113*, 9256.

(29) Perdew, J. P.; Chevary, J. A.; Vosko, S. H.; Jackson, K. A.; Pederson, M. R.; Singh, D. J.; Fiolhais, C. *Phys. Rev. B* **1992**, *46*, 6671–6687.

(30) White, J. A.; Bird, D. M. *Phys. Rev. B* **1994**, *50*, 4954–4957.

(31) Botes, F. G.; Breman, B. B. *Ind. Eng. Chem. Res.* **2006**, *45*, 7415–7426.

(32) Krishnamoorthy, S.; Li, A.; Iglesia, E. *Catal. Lett.* **2002**, *80*, 77–86.

(33) Iglesia, E.; Reyes, S. C.; Madon, R. J.; Soled, S. L. *Adv. Catal.* **1993**, *39*, 221–302.

(34) Cortright, R. D.; Dumesic, J. A. *Adv. Catal.* **2001**, *46*, 161–264.